Coastal Dynamics 2017
Paper No. 075

POROUS MEDIA AND IMMERSED BOUNDARY HYBRID-MODELLING FOR SIMULATING FLOW IN STONE COVER-LAYERS

Bjarne Jensen[1], Xiaofeng Liu[2], Erik Damgaard Christensen[3] and Johan Rønby[4]

Abstract

In this paper we present a new numerical modelling approach for coastal and marine applications where a porous media conceptual model was combined with a free surface volume-of-fluid (VOF) model and an immersed boundary method (IBM). The immersed boundary model covers the method of describing a solid object in a simple computational mesh without resolving the object with a conventional body-fitted mesh. This model enables a detailed resolution of some parts of a stone cover layer for erosion protection with the IBM model while other parts are handled with the conceptual porosity model. In this paper, the model is applied to investigate two practical cases in terms of a cover layer of stones on a flat bed under oscillatory flow at different packing densities, and a rock toe structure at a breakwater.

Key words: Erosion protection, porous media modelling, immersed boundary method, Navier-Stokes equations, OpenFOAM

1. Introduction

In this paper, we present a new numerical modelling approach for coastal and marine applications where a porous media conceptual model was combined with a free surface volume-of-fluid (VOF) model and an immersed boundary method (IBM). With chancing climate conditions, more frequent occurrences of storms, and rising sea level the environmental loads on coastal areas are increasing. Areas which are already protected against erosion needs to be re-evaluated for optimizing the protection strategy. New areas without previous measures against costal erosion becomes relevant for establishing protection against severe erosion of the beach. With the capacity of computational resources that exists today, it is relevant to address the need for computational models that can handle the detailed processes of interaction between stone and rock materials, and the finer sand fractions of the seabed and beaches.

In recent years, numerical methods and computational resources have developed to a level at which consulting and design engineers apply numerical simulations as an integrated part of the design and development process. However, a complete resolution of the porous structure in cover stone layers and breakwaters is not yet feasible. Therefore, a common procedure is to apply resistance-type models where the effect of the stones is added as a source term in the momentum equation. Examples of this were seen in van Gent (1995) where a model based on the Navier-Stokes equations was developed. The porous media, consisting of a rigid skeleton and pores, was treated as one continuum which exerts forces on the fluid due to drag, friction, and acceleration. Several developments have applied the same methodology for two-dimensional domains, e.g., Liu et al. (1999), Hsu (2002), Garcia et al. (2004), and Lara et al. (2006). del Jesus et al. (2012) and Lara et al. (2012) presented a model where also three-dimensional flows were considered. Recently, Jensen et al. (2014) presented a detailed investigation of the theoretical background of the porous media equations and resistance coefficients. These models provide results at the same level of

[1]DHI, Agern Allé 5. DK-2970 Hørsholm, Denmark. bjj@dhigroup.com
[2]Department of Civil and Environmental Engineering, Penn State University, 223B Sackett Building, University Park, PA 16802. xliu@engr.psu.edu
[3]Fluid Mechanics, Coastal and Maritime Engineering, Department of Mechanical Engineering, Technical University of Denmark, DK-2800 Kgs. Lyngby, Denmark. edch@mek.dtu.dk
[4]DHI, Agern Allé 5. DK-2970 Hørsholm, Denmark. jro@dhigroup.com

detail as corresponding physical experiments such as reflection and transmission, overtopping and front slope velocities for stability evaluation, etc.

If the actual armour stones could be resolved directly in the numerical model a higher degree of detail could be achieved. This would correspond to measuring the forces directly at an armour stone as in Moghim et al. (2012). However, the complex geometrical layout of multiple armour stones e.g. in the front layer of a breakwater gives a complicated computational mesh. A traditional way of including solid structures in a computational model is by a body-fitted mesh where the grid cells follow the surface of the structure. For randomly placed armour stones with complicated shapes this may be an impossible or at least a very time-consuming task. Here the immersed boundary method provides an efficient way of including complex shapes in a simple computational mesh.

The immersed boundary method was originally developed to simulate blood flow. Here the entire simulation was performed on a simple Cartesian grid, which did not conform to the shape of, e.g., the heart. Since this first introduction of the method, several modifications and new developments have been presented. In Mittal and Iaccarino (2005) a general overview of the different methods was given. The general idea of the method is to impose the effect of the solid structure into the computational mesh without actually including the structure. In the present model, we applied a discrete forcing approach using ghost cells. The method was described in e.g. Ghias et al. (2007), Mittal et al. (2008), Nasr-Azadani and Meiburg (2011) and Liu (2013). The implementation and derivation of boundary conditions for this model was shown in Jensen (2014).

Some previous examples are seen regarding the application of the immersed boundary method for coastal engineering. Petit et al. (1994) presented a model where virtual velocities were applied to simulate an impermeable sloping bed. Shen and Chan (2010) applied an immersed boundary model to investigate flow around vertical pipelines near a bed and tsunami events initiated by a moving bed. In Peng et al. (2012) an immersed boundary method was applied for simulating the interaction between free surface water waves and submerged objects. Ha et al. (2014) applied the immersed boundary method for simulating the run-up processes of solitary waves where the sloping bed was resolved by the immersed boundary. In Koutrouveli and Dimas (2014) the wave interaction with a fully submerged breakwater was simulated, however, the breakwater was included as an impermeable structure.

The combination of the immersed boundary with a porous media model was shown in van Gent et al. (1994) where the model by Petit et al. (1994) was extended to include porous media. However, applications involving both impermeable structures by the immersed boundary method and porous media were not presented. In Nielsen et al. (2013) the immersed boundary method was combined with a porous media model for simulating the flow in a scour protection around offshore wind turbine foundations. The combination of the immersed boundary method and porous media modelling, including free surface water waves, for detailed simulation of flow around armour stones on breakwaters has, to the authors' knowledge, not previously been presented. Our goal with this work was to combine all three model types, i.e., free surface water waves, porous media, and immersed boundary, in one modelling framework.

The remainder of this paper is organized as follows. In Section 2 the numerical model is described with the modifications for handling the combined porous media flow and immersed boundary method. The model is validated in Section 3 with special emphasis on the immersed boundary implementation. Section 4 presents an example where the forces on natural rock stones on a flat bed are investigated in oscillating flow. Section 5 presents an application with a breakwater rock toe where the fully coupled hybrid model is applied. Final conclusions are given in Section 6.

2. Model Description

The Navier-Stokes equations were solved with an additional body force term to accommodate the effect of the immersed boundaries. The numerical method was based on a finite volume discretization on a collocated grid arrangement.

The first modification of the Navier-Stokes equations was introduced in order to handle the flow in porous media where a direct resolution of the grains and pores is not possible. Here, a volume averaging of the equations was performed in order to derive the VARANS equations. A detailed description of the derivation and implementation of the model was given in Jensen et al. (2014).

The second modification of the Navier-Stokes equations was the introduction of the immersed boundary method. We based the IBM-model on a discrete forcing approach applying ghost cells. The method was described in e.g. Ghias et al. (2007), Mittal et al. (2008), Nasr-Azadani and Meiburg (2011) and was also applied in Liu (2013). The solid boundary was imposed via ghost cells by a body force term included on the right-hand side of the momentum equation (eq. (2)). The details on the derivation of the immersed boundary forcing term in this model was given in Jensen (2014).

The final version of the Navier-Stokes equations was formulated as the continuity equation:

$$\frac{\partial \langle \overline{u}_i \rangle}{\partial x_i} = 0 \tag{1}$$

and the momentum equation:

$$(1 + C_m)\frac{\partial}{\partial t}\frac{\rho \langle \overline{u}_i \rangle}{n} + \frac{1}{n}\frac{\partial}{\partial x_i}\frac{\rho \langle \overline{u}_i \rangle \langle \overline{u}_j \rangle}{n} = -\frac{\partial \langle \overline{p} \rangle^f}{\partial x_i} + g_j x_j \frac{\partial \rho}{\partial x_i} + \frac{1}{n}\frac{\partial}{\partial x_j}\mu\left(\frac{\partial \langle \overline{u}_i \rangle}{\partial x_j} + \frac{\partial \langle \overline{u}_j \rangle}{\partial x_i}\right) - F_i + B_i \tag{2}$$

where ρ is the density of the fluid, u_i is the Cartesian velocity vector $u_i = (u,v,w)$, p is the excess pressure, g_j is the j^{th} component of the gravitational vector, μ is the dynamical viscosity, t is the time, and x_i are the Cartesian coordinates.

Due to the volume averaging procedure, the following changes were introduced. C_m is the added mass coefficient to take the transient interaction between grains and water into account, $< >$ denotes the volume averaged ensemble averaged quantities over the total control volume including the solids of the porous media, $< >^f$ denoted the volume average over the pore volume, in this case applied for the pore pressure. An additional term on the right-hand side, F_i, was included to take account of the resistance force due to the presence of the porous media. The extended Darcy-Forchheimer equation was applied to represent the resistance force that includes linear and non-linear forces as well as inertia forces to account for accelerations.

Due to the introduction of the immersed boundary method the last term on the right hand side, B_i, was introduced. The body force was determined by a first-order temporal discretization of the Navier-Stokes equations.

The governing equations were solved with the PISO algorithm (Pressure Implicit with Splitting of Operator). The details of the PISO algorithm can be found in Issa (1986). It is noted that the body force was determined as an explicit solution only based on known values from the current time step and that the calculation of the body force was included before the momentum predictor step and it was not updated in the corrector step. Ideally, the updating of the body force should be placed inside the PISO loop and an iteration is needed to ensure a tight coupling and convergence. We did not explore this option further in this paper because the time-step in the PISO algorithm is usually small, which makes the explicit treatment of the body force sufficient.

3. Validation of the Immersed Boundary Method

A number of test cases validated the numerical model. The implementation of wave generation and modelling of free surface water waves was validated in detail in Jacobsen et al. (2012) and Paulsen et al. (2014), among others. The porous media implementation was derived and validated in Jensen et al. (2014). The immersed boundary implementation was described and validated with several standard test cases in Jensen (2014). In this paper, we focus on a brief description of the validation of the immersed boundary implementation, which is the third and latest model component in the new hybrid model.

The flow past a circular cylinder was simulated for low Reynolds numbers where the boundary layer and wake were laminar, hence no turbulence closure was applied. The flow over a sphere for high Reynolds numbers was simulated including the LES turbulence closure model. In addition, the interaction between the free water surface and the immersed boundary was validated by simulating the run-up of regular waves around a vertical cylinder in Jensen (2014). Here, a grid refinement and convergence test was also performed to evaluate the required resolution of the computational mesh and the accuracy of the solver.

3.1 *Unidirectional Flow Past a Cylinder*

The flow past a circular cylinder is a basic test case that has been widely used for testing the validity of numerical solvers. This example has also been used previously for validations of the immersed boundary method, see for example Sun et al. (2010), Chiu et al. (2010), Mittal et al. (2008), and Choi et al. (2007). For low Reynolds numbers below 200 the flow can be treated as two-dimensional and laminar. Hereby the model's general ability to reproduce flow and pressure around a solid object can be investigated without the complexity of turbulence modelling. For Re<40 the flow is symmetric while at Re>40 vortex shedding occurs. Simulations were performed for Re=[40;60;80;100;120;160].

The cylinder had a diameter of D=0.4m. The model domain was set up with a transverse and longitudinal dimension at 50D. The upstream distance from the centre of the cylinder to the inlet boundary was 10D. The mesh aspect ratio was 1 in the entire domain. Mesh refinement was applied in areas around the cylinder. The largest grid cell dimension was 0.1m while the smallest dimension around the cylinder was 0.625cm corresponding to 64 grid cells per diameter, D. Regarding the spatial resolution further details are given in Jensen (2014) where a grid convergence test for the present test case was presented. A total of 68,000 grid cells were applied. The mesh is presented in Figure 1 with a close-up of the local mesh refinement around the cylinder.

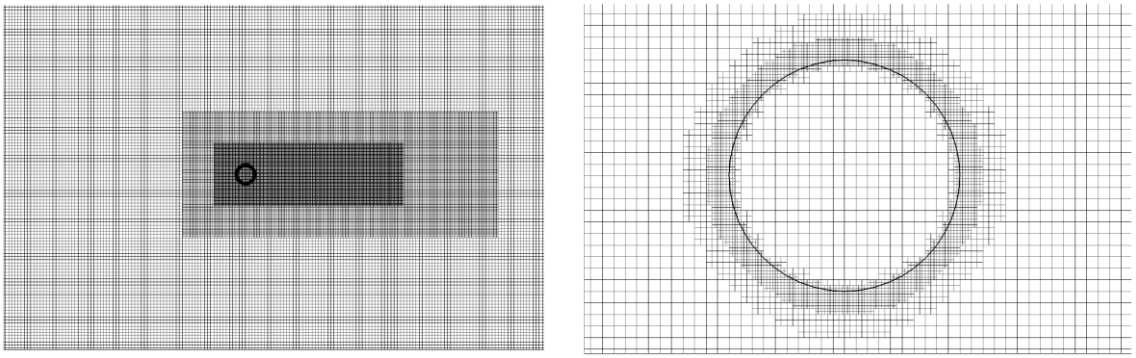

Figure 1. Left panel: Grid for 2D cylinder with refinement zones. Right panel: Close-up of grid near the cylinder surface.

At the inlet boundary a Dirichlet condition was applied for the velocity while a Neumann condition was applied for the pressure. At the sides parallel to the flow direction a slip condition was applied for the velocity while the pressure was given as a Neumann condition. At the outlet boundary the velocity was given as a Neumann condition while a Dirichlet condition was applied for the pressure.

For Re=[40;100] comparisons were made with data for the pressure coefficient along the cylinder surface given in Park et al. (1998), Kim et al. (2001), and Dennis and Chang (1970). For all tested Re-numbers comparisons were made for the Strouhal number with experimental data given in Williamson (1989) and the base suction pressure coefficient, $-C_{pB}$, at the trailing edge with data given in Williamson and Roshko (1990).

Figure 2 shows the pressure coefficient, C_p, along the cylinder half periphery where 0^o corresponds to the upstream leading edge and 180^o corresponds to the downstream trailing edge. For Re=40 the flow was stationary with two symmetrical separation zones downstream the cylinder. For Re=100 laminar vortex shedding was seen with a vortex street downstream the cylinder. In both cases the pressure distribution along the surface of the cylinder was estimated with good agreement with the results given in Park et al. (1998), Kim et al. (2001), and Dennis and Chang (1970). The vortex shedding frequency, represented by the Strouhal number, was also estimated with good accuracy.

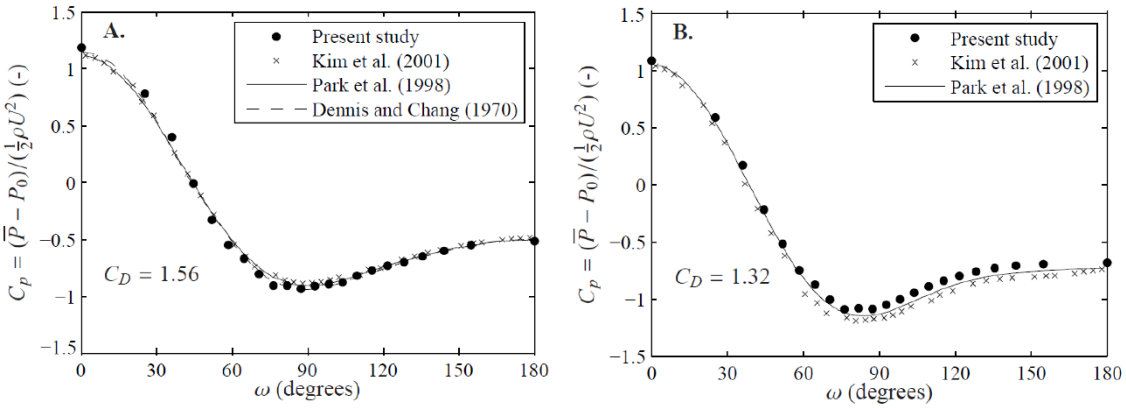

Figure 2. Pressure coefficient on the surface of the cylinder. A: Re=40. B: Re=100.

3.2 *Unidirectional Flow Past a Sphere*

For high Reynolds numbers the flow becomes turbulent and may therefore not be treated as two-dimensional. For validation of the immersed boundary method for three-dimensional high Reynolds numbers flow, a sphere was simulated at high Reynolds numbers. The Smagorinsky LES model was applied for the turbulent closure. In order to address the effect of including the turbulent closure a corresponding simulation was performed without the LES model. The simulations were performed for $Re=1.62 \cdot 10^5$ corresponding to the experimental data presented in Achenbach (1972).

The sphere had a diameter of D=1.0m. The model domain was set up with a transverse and longitudinal dimension of 40D. The upstream distance from the centre of the sphere to the inlet boundary was 10D. The mesh aspect ratio was 1 in the entire domain. Mesh refinement was applied in areas around the sphere. The largest grid cell dimension was 0.3m while the smallest dimension around the sphere was 0.019m. A total of 493,000 grid cells were applied.

At the inlet boundary the velocity was specified as a Dirichlet condition while a Neumann condition was applied for the pressure. At the sides parallel to the flow direction a slip condition was applied for the velocity while the pressure was given as a Neumann condition. The outlet boundary was specified with a Neumann condition for the velocity and a Dirichlet condition for the pressure. Figure 3 present the flow field around the sphere in terms of the velocity and pressure contours.

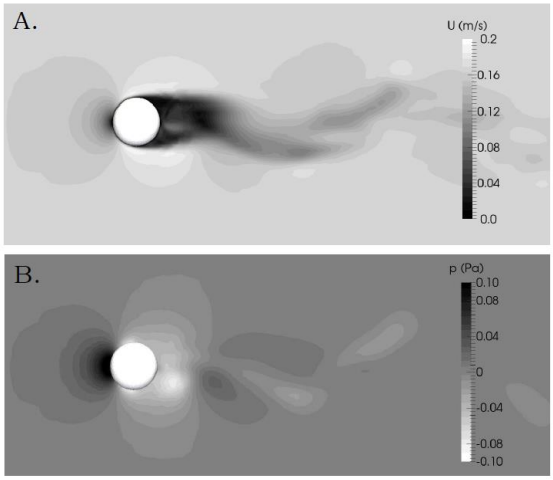

Figure 3. Flow field around the sphere at $Re=1.62 \cdot 10^5$. A. Velocity contours. B. Pressure contours.

Figure 4 (left panel) presents the distribution of the pressure coefficients averaged over 10 minutes compared with data given in Achenbach (1972). The model was found to provide a good representation of

the pressure distribution around the sphere. Especially it is noted that the pressure on the downstream side of the sphere and the base pressure at 180° was well predicted. This implies that the flow separation was estimated correctly as the downstream and base pressure is sensible to the position of the separation point.

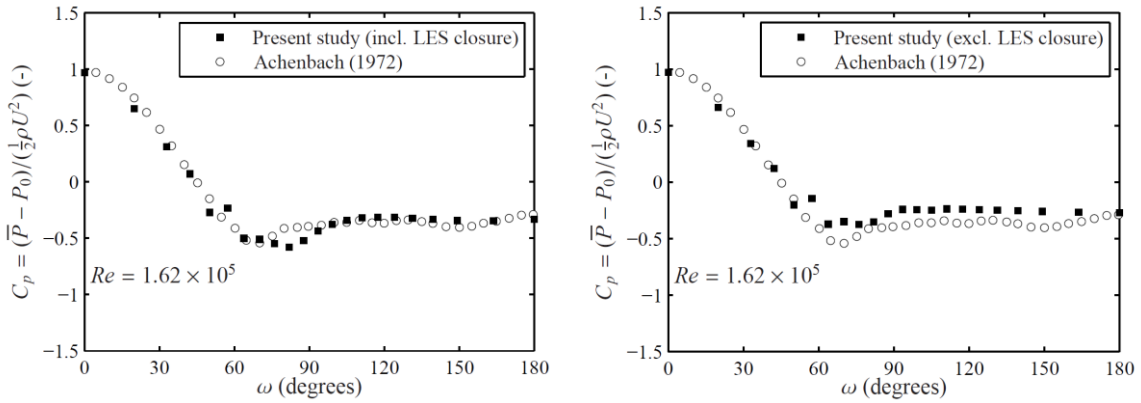

Figure 4. Pressure coefficient on the surface of the sphere at Re=1.62·10^5. Left Panel: Turbulent closure included in terms of the Smagorinsky LES model. Right panel: No turbulence closure.

For the results shown in Figure 4 (left panel) the LES model was applied. The effect of the LES model was addressed by a repetition of the simulation where no turbulence closure was applied. Figure 4 (right panel) presents the results where it is seen how the pressure from about 60° and further downstream was higher than the experimental measurements. The pressure drop is caused by the accelerating flow from 0°-90°. When the flow separates from the surface of the sphere the negative pressure at this point continues around the sphere. In this case, where the pressure was too high it indicates that the separation point was positioned too far upstream compared to the position in the measurements. Hereby the pressure has not decreased sufficiently before the separation occurs.

The comparison between the solution with and without the LES turbulence closure shows that a better solution was obtained by applying the LES model. It should be noted that a detailed verification of the LES model in relation to the IBM implementation is recommended. This is part of the future work planned for the present model development.

4. Stability of Erosion Protection on a Flat Bed

In this example, we show how the model can be used to evaluate the lift force on erosion protection cover stones as function of the packing density and the KC-number. The force variation was found for the individual stones when exposed to an oscillating flow. The same simulation was repeated with stones placed with two different packing densities defined as dense packing with a distance between the stones of approximately one stone diameter, and sparse packing with a distance of approximately 2 diameters between the stones. These two packing densities were repeated at three KC-numbers.

A number of natural stones were mapped in a 3D scanner to obtain a digital representation of the surface of the stones. The stones were selected from the hydraulic laboratory at DTU and the scanning was performed at Texas University at San Antonio (UTSA). To achieve a random packing of the stones the method referred to as bullet physics (http://www.bulletphysics.com) was applied to place the stones randomly on the bed.

Figure 5 shows the stones in the final placement used for the simulations. The stones had a diameter of d_n=1.0m which was achieved by scaling the stones based on the volume of each stone. A total of 17 stones covered an area with a horizontal dimension of (5.6 x 5.6) m for the dense packing density and (7.6 x 7.6) m for the sparse packing density. A hexahedral base mesh was applied with a uniform cell size of 0.2m and an aspect ratio of 1. Two rectangular refinement zones were applied around the stone bed. Furthermore, an additional refinement level was applied locally around the immersed boundary, which provided a resolution

around the stones of 0.025m. A total of 1.1M grid cells were applied for the dense packing and 1.5M grid cells for the sparse packing. The area covered with stones was relatively small, however, periodic boundary conditions were applied in order to simulate the effect of a larger area being covered with stones.

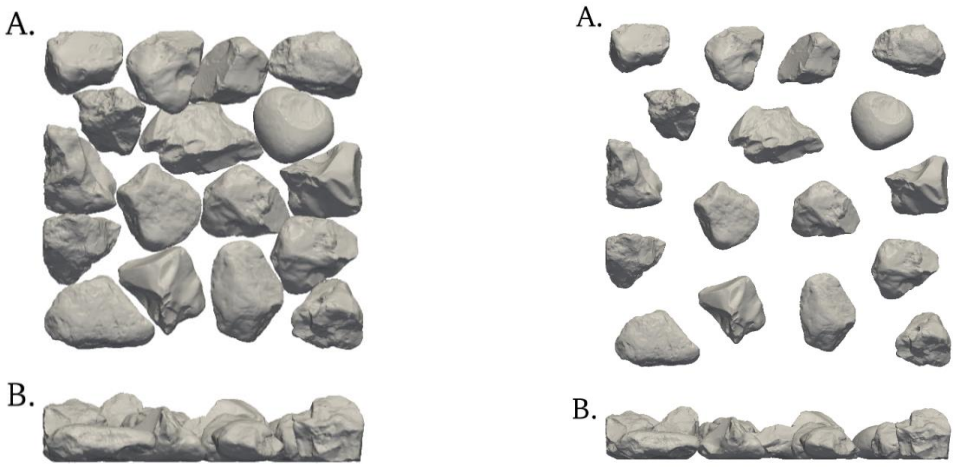

Figure 5. Natural stones randomly placed on an impermeable bed. A. Plan. B. Section view. Left panel: dense packing. Right panel: sparse packing.

The oscillating flow was generated by a body force introduced in the momentum equation. Hereby, the flow was driven to a sinusoidal motion with periods of T=[4;8;12]s and a maximum velocity at U_m=1m/s. This corresponds to KC=[4;8;12] based on the stone diameter. The model provides the forces on each stone in three dimension. From this, it is possible to investigate the variability of the forces between the individual stones and it becomes obvious that important parameters are the individual shape, placement, and orientation of the stones. In this paper, the results are condensed into an exceedance probability plot for the lift forces, which is expressed as an average of the exceedance curves for all stones. In this way, it is possible to evaluate the effect of the packing density and the KC-number as a whole for the entire layer of cover stones.

Figure 6 shows the exceedance probability of the positive lift force for the three KC-numbers and for the dense and sparse packing density, respectively. At the dense packing the effect of the KC-number was found to be small, i.e., the maximum lift force was similar at all tested KC-numbers. By examining the details of the flow field, it was seen that the dense packing prevented different flow regimes to develop at the different KC-numbers hence eliminating the KC-effect on the lift force.

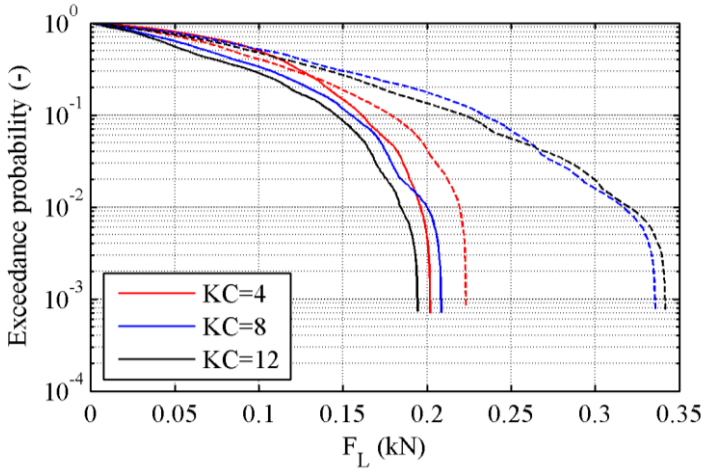

Figure 6. Mean exceedance probability on the lift force for dense and sparse packing densities at three KC-numbers. Full line: dense packing. Dashed line: sparse packing.

The effect of the packing density was found to be most pronounced at the two highest KC-numbers. At the sparse packing density the maximum lift force increased with approximately 68% compared to the dense packing. This was not the case for the lowest KC-number where the lift force only increased with approximately 10%. At the low KC-number the amplitude of the oscillation was so small that the flow around one stone only interfered very little with the neighboring stones, both at the dense and sparse packing. For the higher KC-numbers the amplitude was large enough for the flow to pass over more than one stone at each oscillation. Therefore, the flow around each stone and the developed flow regimes were affected by the distance from one stone to the neighboring stone.

5. Stability of a Breakwater Rock Toe Structure

As the second example, a rubble mound breakwater rock toe was simulated with the full hybrid model. The breakwater core, filter and main armour layers were simulated with the porosity model while the rock toe was resolved with the immersed boundary model. The stability of the toe structure of a breakwater is of general interest regarding the overall stability of the structure. The toe acts as support for the main armour layer as well as protection against scour. Some recent examples of investigations of rock toe stability were presented in Muttray (2013) and van Gent and van der Werf (2014). Stability formulas were derived based on model experiments taking into account the effect of, e.g., toe dimension, wave steepness and water depth. This example shows how the hybrid model can be applied to investigate the toe stability as a function of the surf similarity parameter. The actual forces on the stones were evaluated as well as the flow in and above the toe.

It is noted that a general investigation of stability would apply irregular sea states based on a defined wave spectrum. This is also apparent from the design formulas in, e.g., Muttray (2013), and van Gent and van der Werf (2014) where spectral quantities for wave heights and periods are applied. In the following it is demonstrated how some details of the physical processes can be investigated by means of the hybrid model. For this, shorter time series of regular waves were applied.

Figure 7 presents the general layout of the breakwater including the toe structure. The breakwater consisted of a core, a filter layer, and an outer armour layer. Both the front and rear side had a slope of 1:1.5. The crest height was 30m and the crest width was 6m.

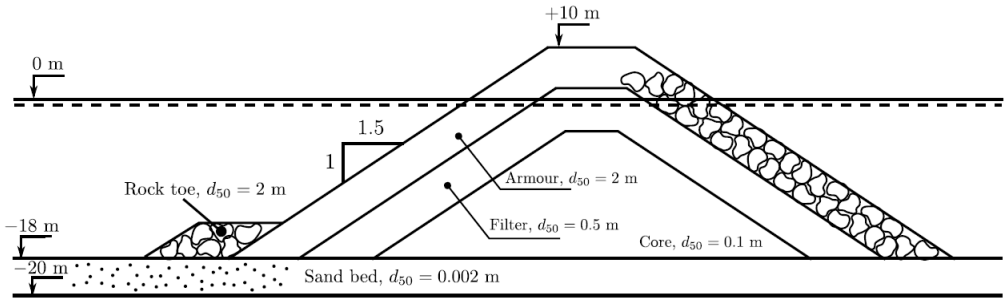

Figure 7. General layout of the breakwater for rock toe simulations.

5.1 *Breakwater Setup*

The main part of the breakwater that consisted of the core, filter, and armour layers was modelled with the porosity model. The characteristics of the individual components of the main breakwater are given in Figure 8. The resistance parameters, α and β, for the porosity model were set to α=500 and β=2.0 according to Jensen et al. (2014).

The computational domain had a dimension of (length x width x height) (800 x 10.5 x 40) m with the breakwater toe positioned at a distance of 600m from the inlet boundary. A hexahedral mesh was applied with a uniform grid spacing in all directions of 0.5m. Grid refinement was applied in a band around the free water surface with one refinement level providing a grid spacing of 0.25m corresponding to 20 points per wave height. The grid around the main breakwater structure was also refined with one refinement level

where the porosity model was applied. Further refinement was applied at the toe structure as described in the following. Including the toe refinement the total number of grid cells was 2,400,000.

Each individual stone in the toe section was resolved in the model. For this, a detailed representation of the stones was needed. A number of natural stones were mapped in a 3D scanner as for the previous example with stones on a flat bed. To achieve a random packing of the stones a six-degree-of-freedom rigid body motion solver was applied to arrange the stones. Again, the libraries by Bullet Physics were used. Here the stones were dropped along an impermeable sloping bed, which gave a natural random placement at the toe of the breakwater. Figure 8 (left panel) shows the final placement of the stones next to the main part of the breakwater that was modelled with the porosity resistance model.

The overall grid was set up with refinement levels around the free water surface and the porous breakwater structure. Three additional refinement levels were applied around the toe structure providing a minimum grid size near the stone surfaces of 3.1cm corresponding to 64 grid cells per stone diameter, d_{50}. This corresponded to the same relative resolution as for the validation case for unidirectional flow past a cylinder in Section 3.1. The computational mesh is shown for a vertical section through the toe structure in Figure 8 (right panel). The grid refinement was optimized with a refinement procedure that detected the solid surface of the stones and applied refinement levels around this surface. As such, the number of grid cells was optimized as the refinement for the smallest grid cells around the stones was only present where it was needed for the immersed boundary.

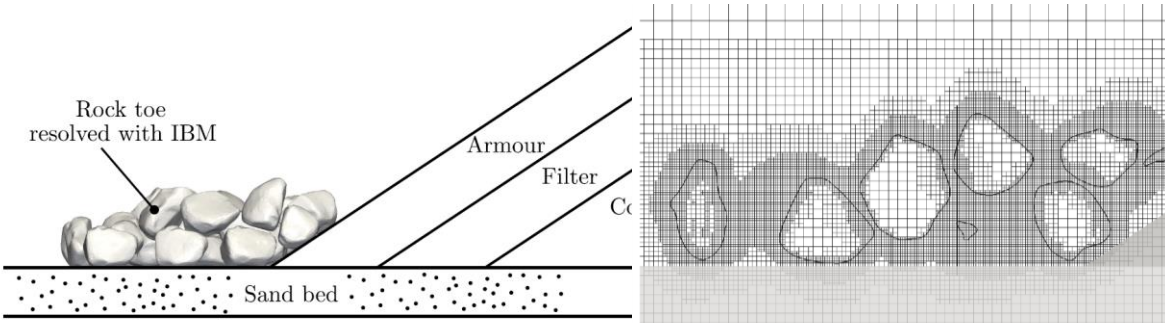

Figure 8. Left panel: Placement of rocks for the toe structure. Right panel: Close-up of grid refinement around the toe rock stones. The outer contours of the stones for the presented vertical section are shown with black lines. The main porous layers of the breakwater and the sand bed are indicated with grey.

5.2 *Wave Conditions*

Regular waves were applied for investigating the forces and loading process. Four wave conditions were simulated with constant wave height and varying wave period as shown in Table 1. The surf similarity parameter, $\xi_0 = \tan(\gamma)/(H_0/L_0)^{1/2}$, was defined in e.g. Battjes (1974) where γ is the slope of the bed, H_0 is the deep water wave height, and L_0 is the deep water wave length. A water depth of h=18m was applied for all simulations. The waves were generated as Stokes 5th order waves by means of relaxation zones according to Jacobsen et al. (2012).

Table 1. Wave conditions for breakwater rock toe simulations.

Wave No.	H (m)	T (s)	ξ_0	Breaker type
1	5.13	6.7	2.31	Plunging
2	5.13	10.1	3.07	Plunging
3	5.13	16.8	4.39	Surging
4	5.13	20.1	5.11	Surging

5.3 *Forces on and Stability of the Rock Toe*

The stones in the toe structure were placed in approximately two layers as shown in Figure 8. The forces were extracted for stones placed in the top and bottom layer. The effect of having two layers was apparent for both wave periods. In the bottom layer, the stones were sheltered and experienced a low lift force. At

the top layer, the stones were exposed to the flow acceleration above the toe that created a large lift force. For stability the top layer is of interest in order to ensure that the destabilizing forces do not exceed the stabilizing forces. Figure 9 shows the flow field around the stones for the wave condition with a wave period of T=20.1s at the instance in time where the largest lift forces occur at the top layer.

The stones experienced similar loading cycle for the different wave lengths. For the stones in the top layer, the loading cycle was oscillating in a regular manner with two positive lift events during one wave period. This was caused by the low pressure above the stone due to flow acceleration both during run-up and run-down. The positive lift force was larger during run-up than run-down. For the stones in the bottom layer, only one positive lift event was found for each wave period. This was associated with the run-up stage while the flow was dampened sufficiently to prevent positive lift during run-down.

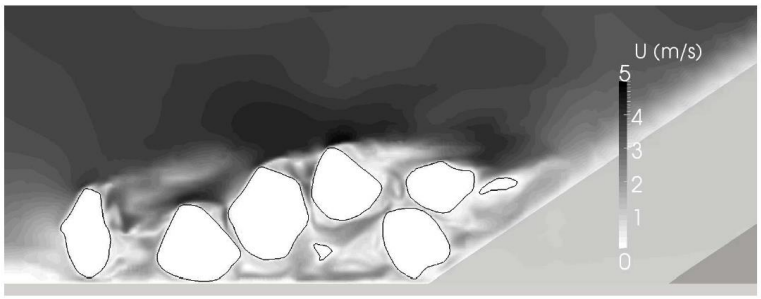

Figure 9 Velocity field for wave period T=6.7s at one instance in time when maximum lift force occurs at the top layer.

In this paper, we have condensed the results into the maximum lift force as function of the surf similarity parameter at the four wave conditions ranging from the plunging to the surging breaker regime. Figure 10 presents the maximum lift force over one wave period. First, it is noted that the lift force increased for increasing surf similarity parameter. This is a result of larger orbital velocities at the bed for larger wave lengths as well as the differences in the run-up and run-down process for the different surf similarity parameters.

Regarding stability, the submerged weight of the stones is indicated in Figure 10 based on the diameter, d_{50}. The simulated wave conditions did not cause lift forces that exceeded the submerged weight of the stones. It is noted that based on the most recent rock toe stability formulas in Muttray (2013) and van Gent and van der Werf (2014) the applied wave conditions should not cause instabilities.

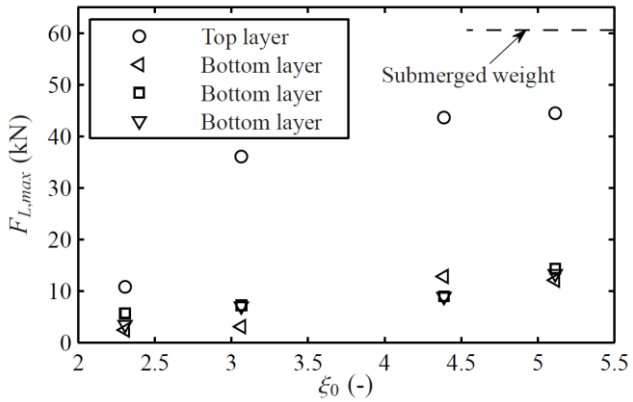

Figure 10. Maximum lift force as a function of the surf similarity parameter, ξ_0. The submerged weight of the stones is indicated based on the diameter, d_{50}.

6. Conclusions

The present paper presents a hybrid modelling approach for coastal engineering problems with two application examples. The new model combines a standard Navier-Stokes solver with a porous media

resistance model and an immersed boundary model for solid structures. The following conclusions are summarized:

1. A discrete forcing procedure for immersed boundary modelling was implemented in the OpenFoam CFD model based on an additional forcing term in the momentum equation.
2. The flow around a 2D cylinder and 3D sphere was represented with good accuracy compared to experimental data.
3. The immersed boundary model was coupled with the porous media resistance model for simulation of solid structures near sand and gravel materials.
4. The possible extent of the model was exemplified by simulation of flow in a stone cover layer on a horizontal bed where the lift force was found to increase with approximately 68% when the distance between the stones was doubled from 1 to 2 stone diameters at the high KC-numbers of 8 and 12.
5. Finally the full hybrid model was used to simulate the loads on a breakwater rock toe structure where the lift forces were found to increase with an increasing surf similarity parameter.

Further work is recommended on this topic. Currently, future work is planned to include a detailed validation of the LES turbulence closure in relation to the IBM method and inclusion of validation cases for stones placed inside porous materials Rigid-body-motion solvers for movements of armour stones are also an area that may be of interest for coastal engineering problems.

Acknowledgments

The first author was supported by the Danish Ministry of Science, Technology and Innovation through the GTS grant: Fremtidens Marine Konstruktioner (Future Marine Structures). The second author was supported by the U.S. Army Corps of Engineers (grant\# W912HZ13P0241) and U.S. Bureau of Reclamation (grant \# R14AC00015). The 3D-scanning of the stones was performed by students at UTSA.

References

Achenbach, E., 1972. Experiments on the flow past spheres at very high Reynolds numbers. *Journal of Fluid Mechanics*, *54*(3), 565.

Battjes, J. A., 1974. Surf similarity. In *International Conference on Coastal Engineering* (pp. 466–480). Copenhagen.

Chiu, P. H., Lin, R. K., & Sheu, T. W. H., 2010. A differentially interpolated direct forcing immersed boundary method for predicting incompressible Navier–Stokes equations in time-varying complex geometries. *Journal of Computational Physics*, *229*(12), 4476–4500.

Choi, J.-I., Oberoi, R. C., Edwards, J. R., & Rosati, J. A., 2007. An immersed boundary method for complex incompressible flows. *Journal of Computational Physics*, *224*(2), 757–784.

Dennis, S. C. R., & Chang, G.-Z., 1970. Numerical solutions for steady flow past a circular cylinder at Reynolds numbers up to 100. *Journal of Fluid Mechanics*, *42*(3), 471–489.

Garcia, N., Lara, J., & Losada, I., 2004. 2-D numerical analysis of near-field flow at low-crested permeable breakwaters. *Coastal Engineering*, *51*(10), 991–1020.

van Gent, M. R. A., Tonjes, P., Petit, H. A. H., & van den Bosch, P., 1994. Wave action on and in permeable structures. In *International Conference on Coastal Engineering* (pp. 1739–1753).

van Gent, M.R.A., 1995. Wave interaction with permeable coastal structures. Ph.D. thesis. Delft University.

van Gent, M. R. A., & van der Werf, I. M., 2014. Rock toe stability of rubble mound breakwaters. *Coastal Engineering*, *83*, 166–176.

Ghias, R., Mittal, R., & Dong, H., 2007. A sharp interface immersed boundary method for compressible viscous flows. *Journal of Computational Physics*, *225*(1), 528–553.

Ha, T., Shim, J., Lin, P., & Cho, Y.-S., 2014. Three-dimensional numerical simulation of solitary wave run-up using the IB method. *Coastal Engineering*, *84*, 38–55.

Hsu, T., 2002. A numerical model for wave motions and turbulence flows in front of a composite breakwater. *Coastal Engineering*, *46*(1), 25–50.

Issa, R., 1986. Solution of the Implicitly Discretised Fluid Flow Equation by Operator-Splitting. *Journal of*

Computational Physics 1, 40-65.
Jacobsen, N. G., Fuhrman, D. R., & Fredsøe, J., 2012. A wave generation toolbox for the open-source CFD library : OpenFoam. *International Journal for Numerical Methods in Fluids*, *70*, 1073–1088.
Jensen, B., Jacobsen, N. G., & Christensen, E. D., 2014. Investigations on the porous media equations and resistance coefficients for coastal structures. *Coastal Engineering*, *84*, 56–72.
Jensen, B., 2014. Wave interaction with porous coastal structures. Ph.D. thesis. Technical University of Denmark.
del Jesus, M., Lara, J. L., & Losada, I. J., 2012. Three-dimensional interaction of waves and porous coastal structures Part I: Numerical model formulation. *Coastal Engineering*, *64*, 57–72.
Kim, J., Kim, D., & Choi, H., 2001. An Immersed-Boundary Finite-Volume Method for Simulations of Flow in Complex Geometries. *Journal of Computational Physics*, *171*(1), 132–150.
Koutrouveli, T. I., & Dimas, A. A., 2014. Numerical simulation of wave propagation over submerged composite breakwaters using the immersed boundary method. In *International Conference on Ocean, Offshore and Arctic Engineering* (pp. 1–9).
Lara, J. L., Garcia, N., & Losada, I. J., 2006. RANS modelling applied to random wave interaction with submerged permeable structures. *Coastal Engineering*, *53*(5–6), 395–417.
Lara, J. L., del Jesus, M., & Losada, I. J., 2012. Three-dimensional interaction of waves and porous coastal structures Part II: Experimental validation. *Coastal Engineering*, *64*, 26–46.
Liu, P. L.-F., Lin, P., Chang, K.-A., & Sakakiyama, T., 1999. Numerical modeling of wave interaction with porous structures. *Journal of Waterways, Port, Coastal and Ocean Engineering*, *125*, 322–330.
Liu, X., 2013. Realistic Flow Simulations around and inside Porous Scour Protections. In *Proceedings of 2013 IAHR Congress* (pp. 1–8).
Mittal, R., & Iaccarino, G., 2005. Immersed Boundary Methods. *Annual Review of Fluid Mechanics*, *37*(1), 239–261.
Mittal, R., Dong, H., Bozkurttas, M., Najjar, F. M., Vargas, A., & von Loebbecke, A., 2008. A Versatile Sharp Interface Immersed Boundary Method for Incompressible Flows With Complex Boundaries. *Journal of Computational Physics*, *227*(10), 4825–4852.
Moghim, M. N., & Tørum, A., 2012. Wave induced loading of the reshaping rubble mound breakwaters. *Applied Ocean Research*, *37*, 90–97.
Muttray, M. (2013). A pragmatic approach to rock toe stability. *Coastal Engineering*, *82*, 56–63.
Nasr-Azadani, M. M., & Meiburg, E., 2011. TURBINS: An immersed boundary, Navier–Stokes code for the simulation of gravity and turbidity currents interacting with complex topographies. *Computers & Fluids*, *45*(1), 14–28.
Nielsen, A. W., Liu, X., Sumer, B. M., & Fredsøe, J., 2013. Flow and bed shear stresses in scour protections around a pile in a current. *Coastal Engineering*, *72*, 20–38.
Park, J., Kwon, K., & Choi, H., 1998. Numerical Solutions of Flow Past a Circular Cylinder at Reynolds Numbers up to 160. *KSME Int. J.*, *12*(6), 1200–1205.
Paulsen, B. T., Bredmose, H., Bingham, H. B., & Jacobsen, N. G., 2014. Forcing of a bottom-mounted circular cylinder by steep regular water waves at finite depth. *Journal of Fluid Mechanics*, *755*, 1–34.
Peng, W., Lee, K.-H., & Mizutani, N., 2012. Application of Direct-Forcing IB-VOF Method to the Simulation of Wave Deformation by Submerged Structures. *Journal of Coastal Research*, *282*(3), 658–670.
Petit, H. A. H., Tonjes, P., van Gent, M. R. A., & van den Bosch, P., 1994. Numerical simulation and validation of plunging breakers using a 2D Navier-Stokes model. In *International Conference on Coastal Engineering* (pp. 511–524).
Shen, L., & Chan, E.-S., 2010. Application of a combined IB–VOF model to wave–structure interactions. *Applied Ocean Research*, *32*(1), 40–48.
Sun, L., Mathur, S. R., & Murthy, J. Y., 2010. An Unstructured Finite-Volume Method for Incompressible Flows with Complex Immersed Boundaries. *Numerical Heat Transfer*, *58*(4), 217–241.
Williamson, C. H., 1989. Oblique and parallel modes of vortex shedding in the wake of a circular cylinder at low Reynolds numbers. *Journal of Fluid Mechanics*, *206*, 579–627.
Williamson, C., Roshko, A., 1990. Measurements of base pressure in the wake of a cylinder at low Reynolds numbers. Flugwiss Welraumforsch 38.